International Journal of Heat and Mass Transfer 128 (2019) 401–417

Contents lists available at ScienceDirect

International Journal of Heat and Mass Transfer

journal homepage: www.elsevier.com/locate/ijhmt

Water functionalized *CuO* nanoparticles filled in a partially heated trapezoidal cavity with inner heated obstacle: FEM approach

Rizwan ul Haq [a,*], Sidra Aman [b]

[a] Department of Electrical Engineering, Bahria University, Islamabad, Pakistan
[b] Department of Mathematical Sciences, UAE University, P.O. Box 15551, Al-Ain, United Arab Emirates

ARTICLE INFO

Article history:
Received 19 May 2018
Received in revised form 15 August 2018
Accepted 20 August 2018

Keywords:
Trapezoidal cavity
Nanoparticles
Inner heated obstacle
Nanofluid
KKL model

ABSTRACT

This frame work is established to investigate the thermal management of free convection enclosed in trapezoidal cavity filled with the water based copper oxide (*CuO*) nanofluid. As nanoparticles volume fraction play a significant role to handle the thermal conductivity of any working fluid, so we have addressed the complex nature real world model that widely used at the industrial level and many other mechanisms. An identical trapezoidal shape cavity is placed inside the big trapezoidal cavity that have three various constraints at the surface (cold, insulated and heated). Since bottom wall of the outer cavity is partially heated so various heated portion tests are applied to analyze the influence of heat transfer within the entire cavity. Aspect ratio that depends upon the size of the inner cavity is also determine. Complete and compatible mathematical model is constructed in the form of nonlinear coupled partial differential equation. These set of equations are characterized under the law of conservation of mass, momentum and energy equation along with the restricted domain of the cavity. Koo and Kleinstreuer-Li (KKL) model is used for effective thermal conductivity and viscosity of the nanofluid. A Galerkin based Finite Element method (FEM) is implemented to attain the suitable results in term of stream function and isotherms within the restricted domain of the cavity. Results are also obtained for velocity and temperature of the nanofluid at vertically mean position of the cavity. The simulations are performed for nanoparticles volume fraction $0 \leqslant \phi \leqslant 0.2$ heated portion length $0 \leqslant L_T \leqslant 1$ aspect ratio $0.5 \leqslant AR \leqslant 3.0$, Rayleigh number $10^4 \leqslant Ra \leqslant 10^{5.7}$, and three heated conditions (cold, adiabatic and hot) for inner trapezium. It is found that flow and thermal field are getting stronger due to increase in Rayleigh number. However, fluid velocity is decreasing with increasing nanoparticles volume fraction ϕ as the fluid is getting dens. Heat transfer rate is decreasing with the increase in ϕ and L_T due to dominant convection.

1. Introduction

Natural convection heat transfer is an essential necessity in industries and engineering processes such as heating/cooling processes, solar power and chemical reactors. Particularly in the engineering applications, convection is commonly visualized in the formation of microstructures during the cooling of molten metals, and fluid flows around shrouded heat-dissipation fins, and solar ponds. It has been the subject of extensive research for the last two decades. Fetecau et al. [1] examined natural convection flow of fractional nanofluids over an isothermal vertical plate with thermal radiation. Al-Mdallal et al. [2] used natural convection for flow due to condensation on a porous vertical plate using extended homotopy perturbation method. Peric [3] studied natural convection in trapezoidal cavities. The numerical study for airflow and heat transfer for low-turbulence buoyancy-driven flow in a rectangular cavity was studied by Lyi and Hasan [4]. Prasad and Kulacki [5] studied heat transfer in rectangular porous cavity and effect of aspect ratio on flow structure numerically. They concluded that heat transfer rate increases when the aspect ratio increases. Wu and Wang [6] studied natural convection in an inclined porous cavity under time-periodic boundary conditions. Simulations were carried out recently by Aparna and Seetharamu [7] for heat transfer flow in trapezoidal cavity using finite element computational technique.

Heat transfer can be enhanced according to the industrial need by varying the boundary conditions, boundary layer turbulence and enhancement in the thermophysical properties of the working fluid. Enhancing the thermal conductivity of carrier fluid by addition of nanoparticles is found to be the best promising method in

* Corresponding author.
E-mail addresses: ideal_riz@hotmail.com, rizwanulhaq.buic@bahria.edu.pk (R.ul Haq).

https://doi.org/10.1016/j.ijheatmasstransfer.2018.08.088
0017-9310/

this regard. Initially, Maxwell [8] introduced the idea of possibility of enhancement of thermal conductivity by using small particles which has some limitations as clogging. Later on, Choi [9] concluded that nanoparticles can increase thermal conductivity of nay working fluid significantly. Kelbinski et al. [10] investigated the four techniques contribute to enhance the thermal conductivity of nanofluids: (i) nanoparticles clustering (ii) heat transport in nanoparticles (iii) Brownian motion (iv) molecular-level layering of fluid/particle interface. Aman et al. [11] studied heat transfer convection flow of Maxwell nanofluid with CNTs nanoparticles. They observed that thermal conductivity and Nusselt number of nanofluids get enhance with increasing volume fraction (Tables 2 and 3 of [11]). Aman et al. [12] studied heat transfer MHD flow of Casson nanofluids along a vertical channel and concluded that fluid flow decreases with increase in volume fraction.

The above studies were carried out on nanofluids experimentally or theoretically in different geometries. However, studies on heat transfer of nanofluids in cavities has been a subject of interest to researchers. Boulahia et al. [13] studied mixed convection heat transfer of *Cu*-water nanofluid in a square cavity with heated cylinders. Thermal management of SWCNT-water nanofluid in a partially heated trapezoidal cavity is recently investigated by Haq et al. [14]. They observed that nanofluids have higher rate of heat transfer compared to base fluid. Velocity of the fluid increases by reducing the length of heated portion but thermal field reduces. Mixed convection nanofluid in a 3D lid-driven trapezoidal cavity with flexible side surfaces and inner cylinder was analyzed by Selimefendigil et al. [15]. Alinia et al. [16] numerically examined mixed convection two phase flow of nanofluid in inclined two-sided lid-driven cavity. Melting heat transfer influence on nanofluid flow inside a cavity is analyzed by Sheikholeslami and Rokni [17]. Sheikholeslami and Sadoughi [18] studied Mesoscopic method for MHD nanofluid with different shapes of nanoparticles inside a porous cavity. Talebi et al. [19] studied mixed convection flow of nanofluid in a square lid-driven cavity. Boulahia et al. [20] numerically investigated heat transfer of nanofluid in a lid-driven cavity. Ben-Cheikh et al. [21] investigated natural convection of water-based nanofluid in a square enclosure with non-uniform heating of the bottom wall.

Natural convection in a trapezoidal enclosure filled with carbon nanotube-EG-water nanofluid was studied by Esfe et al. [22]. Job and Gunakala [23] investigated MHD mixed convection flow of nanofluids through a grooved channel with internal solid cylinders. They used Au-water and SWCNT-water nanofluid and found that groove area and shape affect fluid flow and temperature. The rate of heat transfer is proportional to Grashof number at higher Hartmann number. In case of SWCNT-water nanofluids the heat transfer rate is higher at higher Reynolds number. Kareem et al. [24] examined unsteady mixed convection heat transfer in a 3D closed lid-driven cavity. Haq et al. [25] recently investigated nanofluid in a partially heated rhombus with square cylinder. They considered *CuO*-water nanofluids inside a rhombus cavity containing a square obstacle and observed that the fluid flow, thermal field and heat transfer rate are strong for bigger values of Rayleigh number. Ismael et al. [26] studied mixed convection in square cavity filled with *CuO*-water nanofluid. Some of the recent research related to heat transfer and fluid flow is discussed in the published work [27–38].

The above literature motivated us to examine natural convection flow of *CuO*-water nanofluids in a cavity with inner heated cavity. The aim of this study is to examine numerically nanofluids flow and heat transfer in a cavity with inner heated cavity. The top wall is adiabatic and inclined walls are cold. The bottom wall is partially heated in the outer cavity. While the inner trapezium walls are considered to be heated.

2. Mathematical framework

Consider a steady two-dimensional flow of water based nanofluid with *CuO* nanoparticles inside a trapezoidal cavity with an inner heated trapezium. The enclosure is filled with Copper oxide-water nanofluid. The bottom wall of outer cavity is partially heated with constant temperature T_h while the inclined walls are cold with constant temperature T_C. The upper wall is insulated while the inner cavity is with heated walls maintained at constant temperature T_h. Natural convection is considered in this problem and flow is induced due to buoyancy force together with the external pressure gradient. Fig. 1 shows full interpretation of the geometry. In Fig. 2 is the mesh generation that helps to attain the more accurate results at various corners of the cavity. For more accuracy and better result, we increase the number of mesh at the corners of the trapezium and near the partially heated portion. The problem is modeled in the form of dimensional governing equations as:

$$\frac{\partial u}{\partial x}+\frac{\partial v}{\partial y}=0, \tag{1}$$

$$\rho_{nf}\left(u\frac{\partial u}{\partial x}+v\frac{\partial u}{\partial y}\right)=-\frac{\partial p}{\partial x}+\mu_{nf}\left(\frac{\partial^2 u}{\partial x^2}+\frac{\partial^2 u}{\partial y^2}\right), \tag{2}$$

$$\rho_{nf}\left(u\frac{\partial v}{\partial x}+v\frac{\partial v}{\partial y}\right)=-\frac{\partial p}{\partial y}+\mu_{nf}\left(\frac{\partial^2 v}{\partial x^2}+\frac{\partial^2 v}{\partial y^2}\right)-g\rho_{nf}\beta_{nf}(T^*-T_C), \tag{3}$$

$$\left(u\frac{\partial T^*}{\partial x}+v\frac{\partial T^*}{\partial y}\right)=\alpha_{nf}\left(\frac{\partial^2 T^*}{\partial x^2}+\frac{\partial^2 T^*}{\partial y^2}\right), \tag{4}$$

where u and v are velocities along x and y directions, respectively. Here T^* is the temperature, P is the pressure and $\rho_{nf}, \mu_{nf}, \beta_{nf}, \alpha_{nf}$ are density, viscosity, thermal expansion coefficient and thermal diffusivity of nanofluid, respectively. The boundary conditions are:

Along the outer cavity:

At the left and right inclined walls:

$$T^*=T_C. \tag{5a}$$

At the bottom wall:

$$\begin{cases} \frac{\partial T^*}{\partial y}=0, & x<aL, \\ T^*=T_h, & x=(L_T)L, \\ \frac{\partial T^*}{\partial y}=0, & x>bL. \end{cases} \tag{5b}$$

At the top wall:

$$\frac{\partial T^*}{\partial y}=0. \tag{5c}$$

At all solid boundaries:

$$u=v=0. \tag{5d}$$

Along the inner cavity:

At all surfaces of the cavity:

$$T^*=T_h. \tag{5e}$$

Thermophysical properties for nanofluids are expressed in the form:

$$\begin{cases} \beta_{nf}=(1-\phi)\beta_f+\phi\beta_p, \\ \rho_{nf}=(1-\phi)\rho_f+\phi\rho_p, \\ (\rho c_p)_{nf}=(1-\phi)(\rho c_p)_f+\phi(\rho c_p)_p, \\ \alpha_{nf}=\frac{k_{nf}}{(\rho c_p)_{nf}}, \end{cases} \tag{6}$$

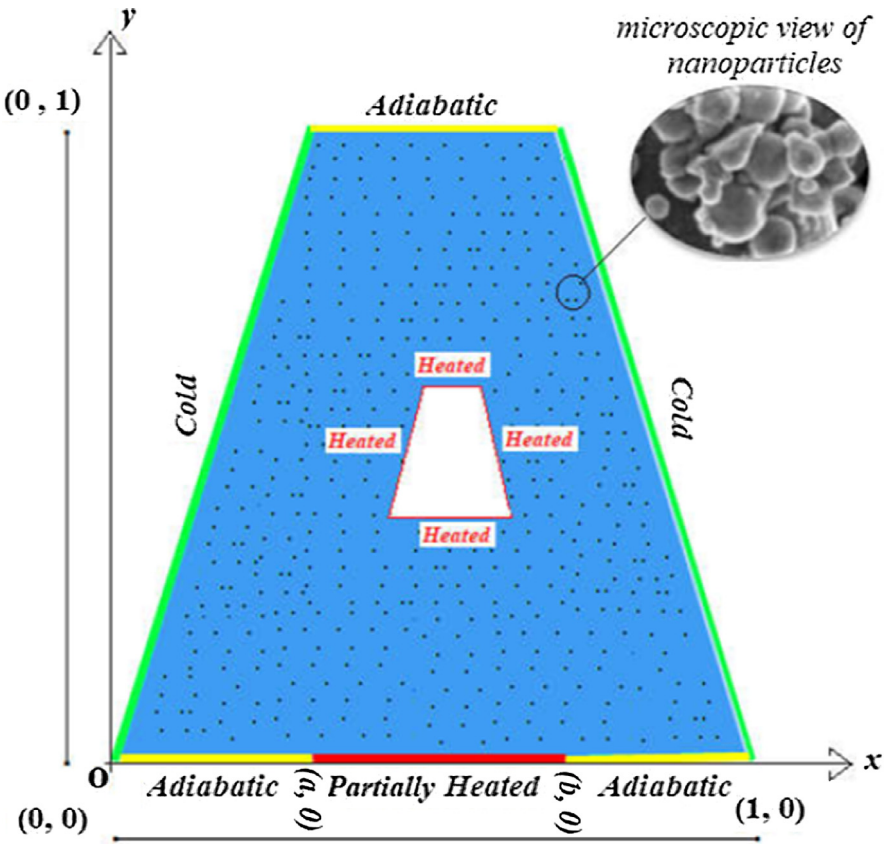

Fig. 1. Geometry of the model.

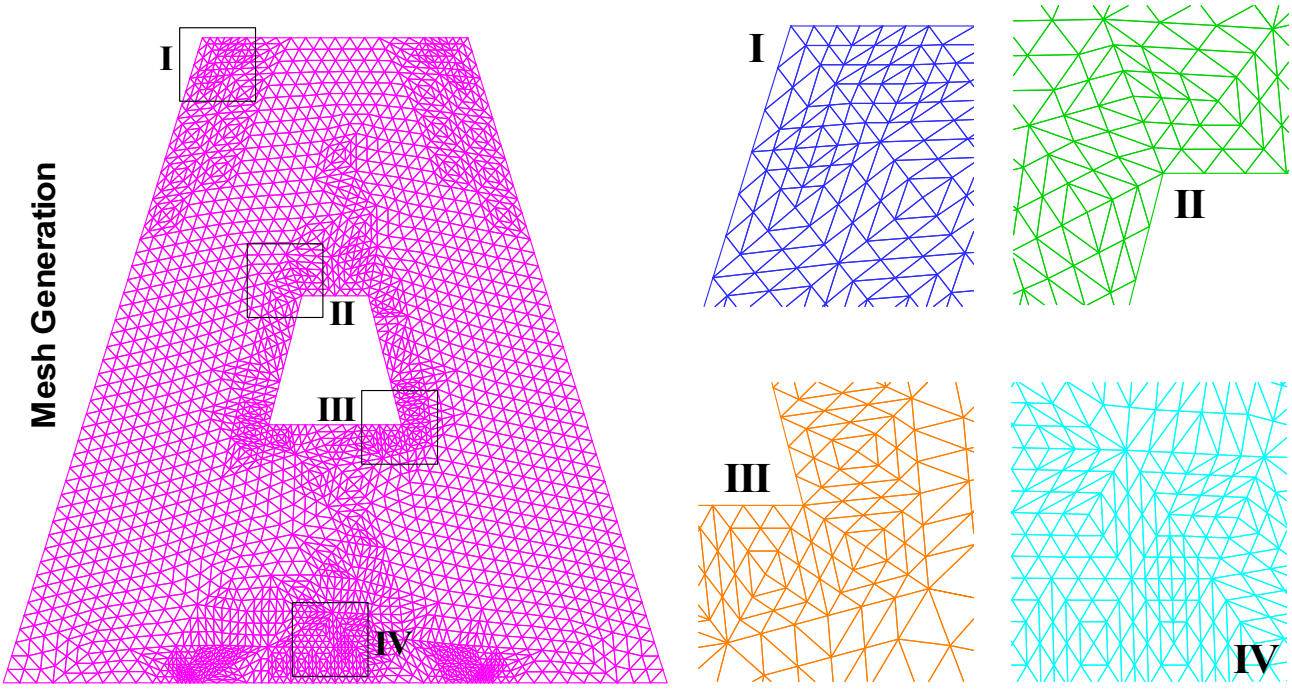

Fig. 2. Mesh generations at different regions of the cavity.

where β_f, β_p, ρ_f, ρ_p, $(c_p)_f$, $(c_p)_p$, are thermal expansion coefficient, density, and specific heat capacity of the base fluid and nanoparticles respectively, which are listed in Table 1. Thermal conductivity model KKL is considered as defined by Koo and Kleinstreuer [39].

$$k_{nf} = k_{static} + k_{Brownian}, \tag{7}$$

where the Static part is defined by Maxwell et al. [40] as follows:

$$\frac{k_{static}}{k_f} = 1 + \frac{3(k_p/k_f - 1)\phi}{(k_p/k_f + 2) - (k_p/k_f - 1)\phi}. \tag{8}$$

The model for dynamic part is employed as defined by Li [42]:

$$k_{Brownian} = 5.10^4 \phi(\rho C_p)_f \sqrt{\frac{\kappa_b T_0}{\rho_p d_p}} \xi'(T_0, \phi, d_p), \quad T_0 = 0.5(T_h + T_c), \tag{9}$$

where $\kappa_b = 1.38 \times 10^{-23}$ J/K is the Boltzmann constant. Here T_0 is the average temperature and d_p is the diameter of nanoparticle. The function ξ for the nanofluid can be defined as follows:

$$\xi'(T_0, \phi, d_p) = (a_1 + a_2 \ln(d_p) + a_3 \ln(\phi) + a_4 \ln(\phi)\ln(d_p) + a_5 \ln(d_p)^2) \ln(T_0) + (a_6 + a_7 \ln(d_p) + a_8 \ln(\phi) + a_9 \ln(\phi)\ln(d_p) + a_{10} \ln(d_p)^2), \tag{10}$$

where the coefficients $a_i (i = 1 \ldots 10)$ are specified in Table 2.

The effective viscosity under the Brownian motion effects can be defined as in [24]:

$$\mu_{nf} = \mu_{static} + \mu_{Brownian} = \mu_{static} + \frac{k_{Brownian}}{k_f} \times \frac{\mu_f}{Pr_f}, \tag{11}$$

where static part of viscosity is given by Brinkman viscosity model [41]:

$$\mu_{static} = \frac{\mu_f}{(1-\phi)^{2.5}}. \tag{12}$$

We utilize the following dimensionless variables in the governing equations:

$$X = \frac{x}{L}, \quad Y = \frac{y}{L}, \quad U = \frac{uL}{\alpha_f}, \quad V = \frac{vL}{\alpha_f}, \quad T = \frac{T^* - T_C}{T_h - T_C}, \quad P = \frac{pL^2}{\rho_f \alpha_f^2}, \quad \nu_f = \frac{\mu_f}{\rho_f}, \quad Pr = \frac{\nu_f}{\alpha_f}, \quad Ra = \frac{\beta_f (T_h - T_C) L^3}{\nu_f \alpha_f}, \tag{13}$$

where Ra and Pr denote the Rayleigh number and Prandtl numbers, respectively. After non-dimensionalization, Eqs. (2)-(4) can be written as:

$$\left(U\frac{\partial U}{\partial X} + V\frac{\partial U}{\partial Y}\right) = -\Psi_1(\phi)\left(\frac{\partial P}{\partial X}\right) + Pr\Psi_2(\phi)\left(\frac{\partial^2 U}{\partial X^2} + \frac{\partial^2 U}{\partial Y^2}\right), \tag{14}$$

$$\left(U\frac{\partial V}{\partial X} + V\frac{\partial V}{\partial Y}\right) = -\Psi_1(\phi)\left(\frac{\partial P}{\partial Y}\right) + \frac{\rho_f}{\rho_{nf}} Pr\Psi_2(\phi)\left(\frac{\partial^2 V}{\partial X^2} + \frac{\partial^2 V}{\partial Y^2}\right) - \Psi_3(\phi) Ra\, Pr T, \tag{15}$$

$$\left(U\frac{\partial T}{\partial X} + V\frac{\partial T}{\partial Y}\right) = \Psi_4(\phi)\left(\frac{\partial^2 T}{\partial X^2} + \frac{\partial^2 T}{\partial Y^2}\right), \tag{16}$$

where

$$\Psi_1(\phi) = \frac{1}{1 - \phi + \phi(\rho_p/\rho_f)}, \quad \Psi_3(\phi) = \frac{1 - \phi + \phi((\rho\beta)_p/(\rho\beta)_f)}{1 - \phi + \phi(\rho_p/\rho_f)},$$

$$\Psi_2(\phi) = \frac{1}{(1-\phi)^{2.5}(1 - \phi + \phi(\rho_p/\rho_f))} + \frac{k_{Brownian}}{k_f Pr_f (1 - \phi + \phi(\rho_p/\rho_f))},$$

$$\Psi_4(\phi) = \frac{1}{1 - \phi + \phi((\rho C)_p/(\rho C)_f)} + \frac{3(k_p/k_f - 1)\phi}{(1 - \phi + \phi((\rho C)_p/(\rho C)_f))(k_p/k_f + 2 - (k_p/k_f - 1)\phi)} + \frac{k_{Brownian}}{k_f(1 - \phi + \phi((\rho C)_p/(\rho C)_f))}.$$

The associated boundary condition are:

At the left and right inclined walls:

$$T = 0. \tag{17a}$$

At the bottom wall:

$$\begin{cases} \frac{\partial T}{\partial Y} = 0, & X < a, \\ T = 1, & X = L_T, \\ \frac{\partial T}{\partial Y} = 0, & X > b. \end{cases} \tag{17b}$$

where L_T is heated length between (a,0) to (b,0). At the top wall:

$$\frac{\partial T}{\partial Y} = 0. \tag{17c}$$

At all solid boundaries:

$$U = V = 0. \tag{17d}$$

At the surface of inner trapezium:

$$T = 1. \tag{17e}$$

The quantity of physical interest Nusselt number for the partially heated domain of trapezium is defined as:

$$Nu_{avg} = \int_{L_T} -\frac{k_{nf}}{k_f}\frac{\partial T}{\partial n} dX, \tag{18}$$

where "n" is the normal direction at the heated surface of trapezium (L_T). For inner heated cavity, length L is replaced by four sides of trapezium L_1, L_2, L_3 and L_4.

3. Numerical procedure

This complex nature model is inspected numerically via Finite Element Method along with the Galerkin technique as defined by Taylor and Hood [43]. By replacing the pressure term with $P = -\gamma\left(\frac{\partial U}{\partial X} + \frac{\partial V}{\partial Y}\right)$, the governing Eqs. (14) and (15) may be written as:

$$\left(U\frac{\partial U}{\partial X} + V\frac{\partial U}{\partial Y}\right) = \gamma\Psi_1(\phi)\frac{\partial}{\partial X}\left(\frac{\partial U}{\partial X} + \frac{\partial V}{\partial Y}\right) + Pr\Psi_2(\phi)\left(\frac{\partial^2 U}{\partial X^2} + \frac{\partial^2 U}{\partial Y^2}\right), \tag{19}$$

$$\left(U\frac{\partial V}{\partial X} + V\frac{\partial V}{\partial Y}\right) = -\gamma\Psi_1(\phi)\frac{\partial}{\partial Y}\left(\frac{\partial U}{\partial X} + \frac{\partial V}{\partial Y}\right) + \frac{\rho_f}{\rho_{nf}} Pr\Psi_2(\phi)\left(\frac{\partial^2 V}{\partial X^2} + \frac{\partial^2 V}{\partial Y^2}\right) - \Psi_3(\phi) Ra\, Pr T, \tag{20}$$

4. Results and discussion

In order to obtain the fluid flow and heat distribution within the cavity, we have plotted the streamlines and isotherms behavior. The heat transfer rate at the surface of the cavity is given by Nusselt number. Numerical simulation is executed for Rayleigh number ($10^4 \leqslant Ra \leqslant 10^{5.7}$), nanoparticles volume fraction ($0 \leqslant \phi \leqslant 0.2$), aspect ratio ($0.5 \leqslant AR \leqslant 3$), partially heated bottom portion ($0.2 \leqslant L_T \leqslant 1.0$) and three different constraints (cold, adiabatic and heated) at the outer surface of inner cavity.

Fig. 3 depicts the behavior of isotherms and streamlines due to cold, adiabatic and heated inner trapezium. In Fig. 3(a)-(c), two symmetric boluses represent the streamlines of the nanofluid. The bolus size increases and spread in the whole cavity when going through cold to hot inner trapezium, the streamlines get stronger. In Fig. 3(d), nanofluid near the heated portion is hotter than the remaining large part which is colder as the inner cavity is cold. In Fig. 3(e), for adiabatic inner cavity, the heat transfer is stronger

Table 1
Thermophysical properties of water and nanoparticles.

Properties	*CuO*	Water
ρ (kg/m^3)	6500	997.1
c_p (J/kg K)	540	4179
k (W/mK)	18	0.613
β (K^{-1})	29	21
d_p (nm)	45	–

Table 2
The coefficient values of nanofluids.

Coefficients a_i	*CuO-water*	Coefficients a_i	*CuO-water*
$i = 1$	−26.5933108	$i = 6$	48.40336955
$i = 2$	−0.403818333	$i = 7$	−9.787756683
$i = 3$	−33.3516805	$i = 8$	190.24561009
$i = 4$	−1.915825591	$i = 9$	10.9285386565
$i = 5$	−0.006421858	$i = 10$	−0.72009983664

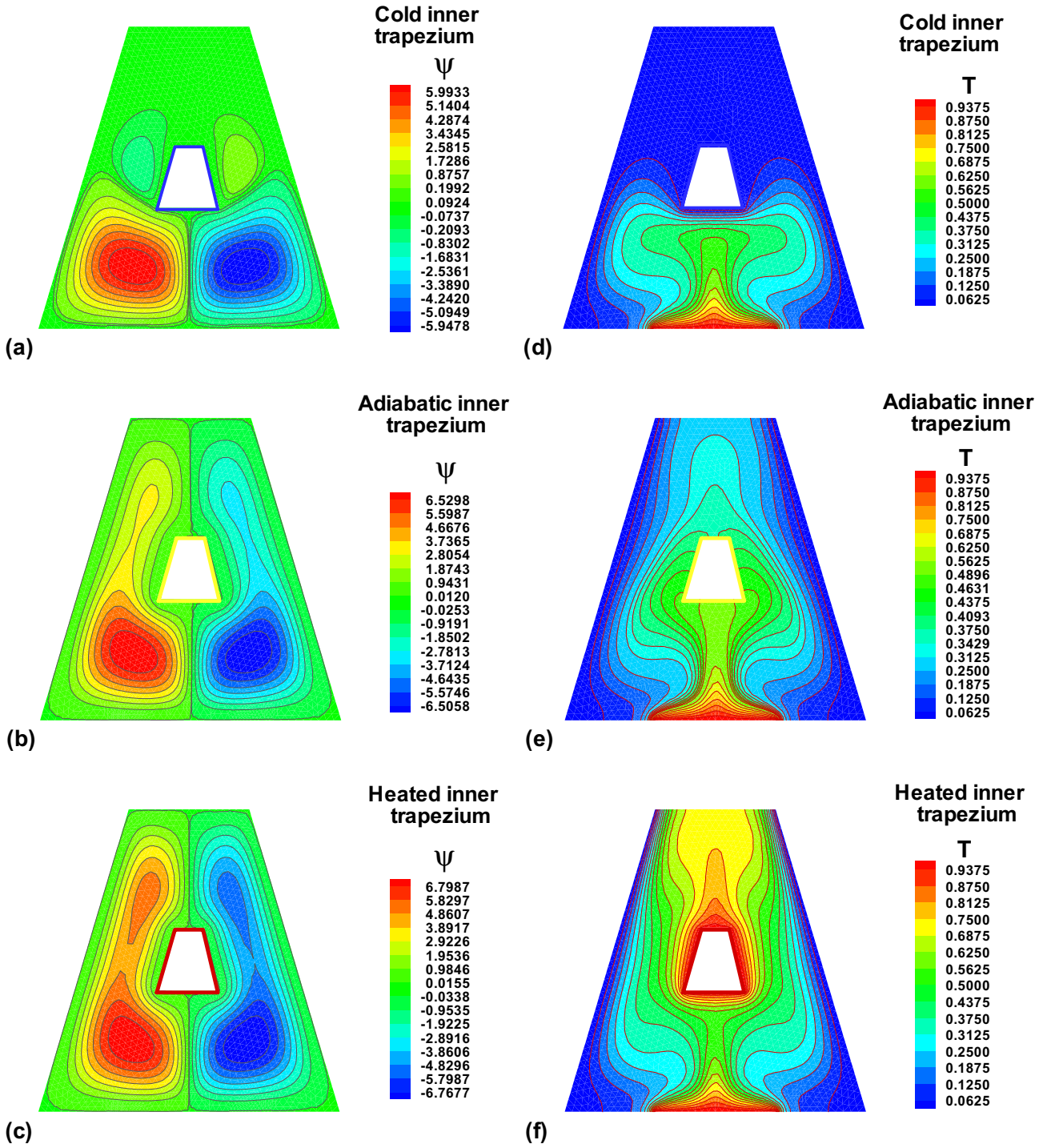

Fig. 3. Variation of (a)-(c) Stream lines ψ and (d)-(f) isotherms for various conditions (cold, adiabatic and heated) defined at the inner trapezium when $L_T = 0.4, \phi = 0.1$ and $Ra = 10^5$.

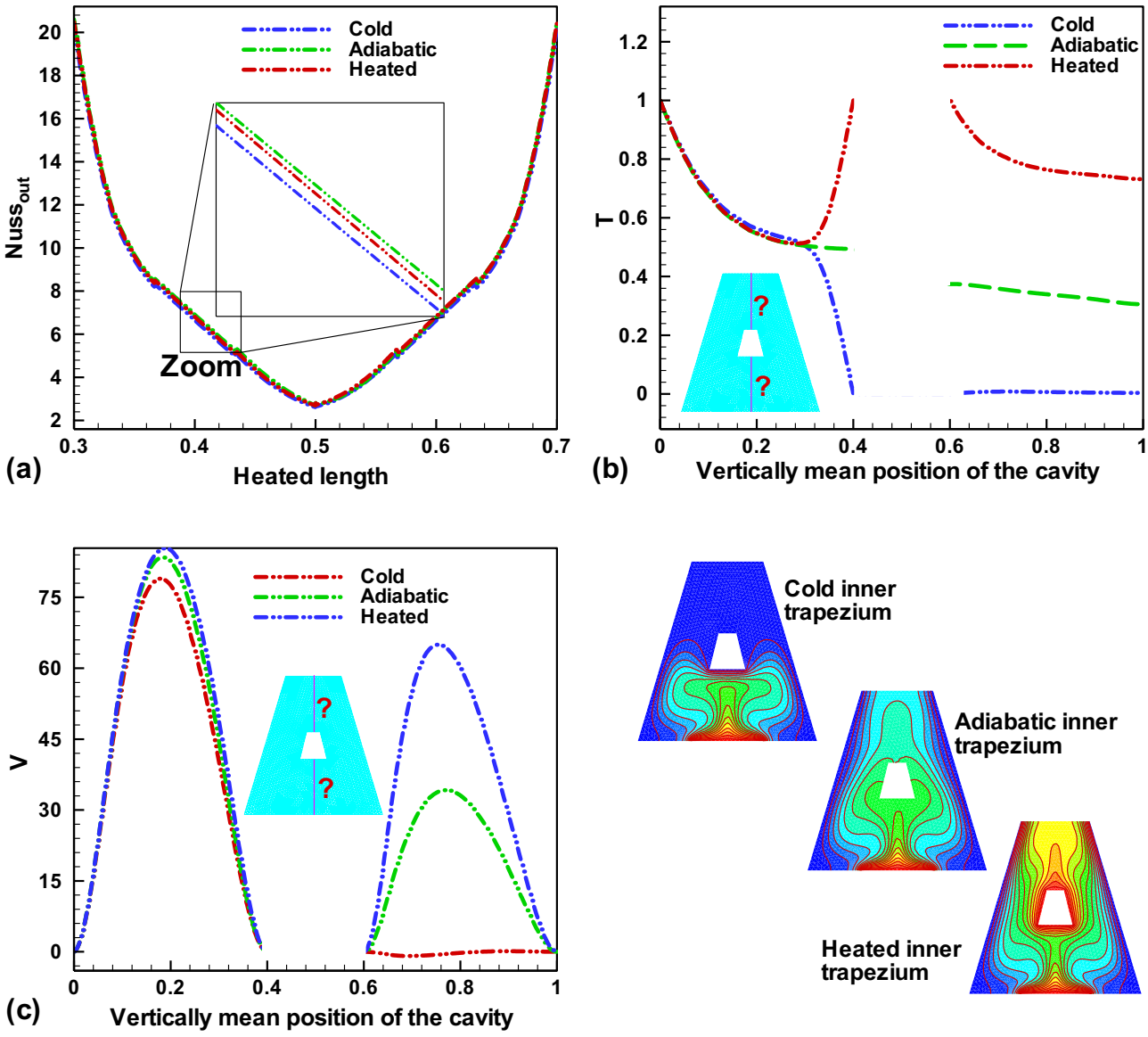

Fig. 4. Variation of (a) Nusselt number at outer cavity, (b) temperature T and (c) velocity V along the vertically mean position for various conditions (cold, adiabatic and heated) defined at the inner trapezium when $L_T = 0.4, \phi = 0.1$ and $Ra = 10^5$.

boluses have larger size compared to Fig. 3(d). In Fig. 3(f), heat spreads in the cavity except the cold inclined walls and makes most of the fluid hot near the heated cavity and partially heated bottom wall.

Variation of Nusselt number of the outer trapezium, temperature and velocity with three kinds of heated conditions are presented in Fig. 4(a)-(f). Fig. 4(a) shows that Nusselt number has highest profile at adiabatic condition following by that of heated inner cavity while it has the lowest profile for cold inner cavity. Moreover, Nusselt number has higher value. For adiabatic inner cavity, Nusselt number is highest. Fig. 4(b) shows temperature profile is increasing while going from cold to heated inner trapezium. Fig. 4(c) depicts that fluid flow increases while going from cold to heated condition of inner trapezium because for heated inner trapezium, most of the fluid is hot and convection augments.

The impact of length of heated portion on isotherms and streamlines are depicted in Fig. 5(a)-(h). The streamlines get stronger in Fig. 5(a)-(d) and bolus size increases as we increase the length of the heated portion. In Fig. 5(e)-(h), with increasing heated portion length the temperature of the fluid increases and isotherms becomes more distorted. The thermal plume near the inner heated cavity is small for $L_T = 0.2$ and spreads towards the upper portion for higher values of L_T. The maximum absolute values for stream function at different lengths are 6.4942 ($L_T = 0.2$), 6.798 ($L_T = 0.4$), 7.786 ($L_T = 0.7$) and 7.862 ($L_T = 1.0$), clearly showing the increasing strength of streamlines with increasing heated length.

Fig. 6(a) shows that the variation of Nusselt number of the inner cavity with the heated length of outer trapezium for various sides of the inner trapezium walls. It is obvious that Nusselt number decreases with increasing length of partially heated side of outer trapezium. When length of heated wall increases, it augments thermal conductivity and conductive heat transfer becomes dominant, due to which Nusselt number reduces. Additionally, we can see that Nusselt number attains a highest value at the bottom wall L_1 while at the top wall of the inner cavity L_3, the variation of Nusselt number is very small as it is far from the heated

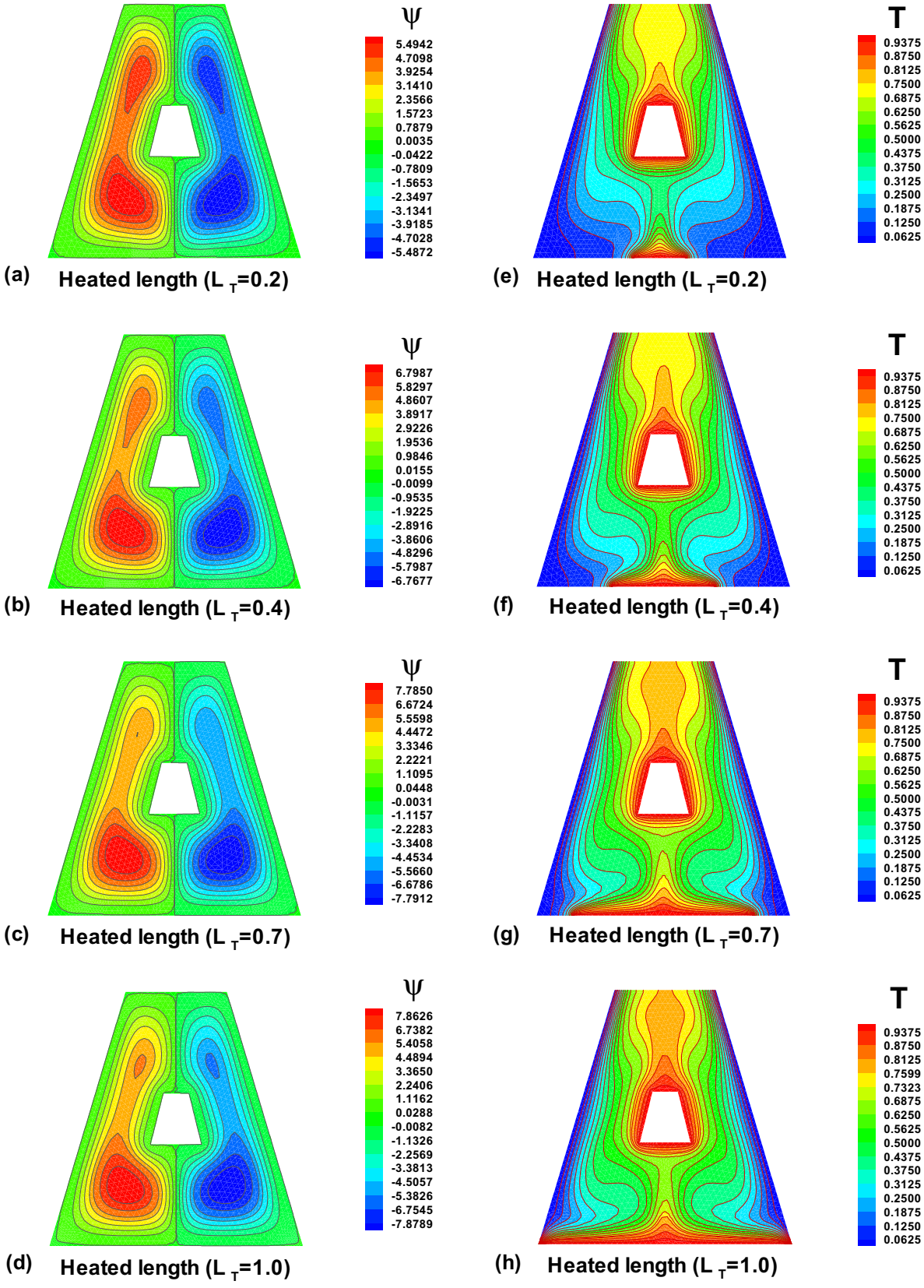

Fig. 5. Variation of (a)-(c) Stream lines ψ and (d)-(f) isotherms T for various heated lengths (L_T) of bottom of the cavity when $\phi = 0.1$ and $Ra = 10^5$.

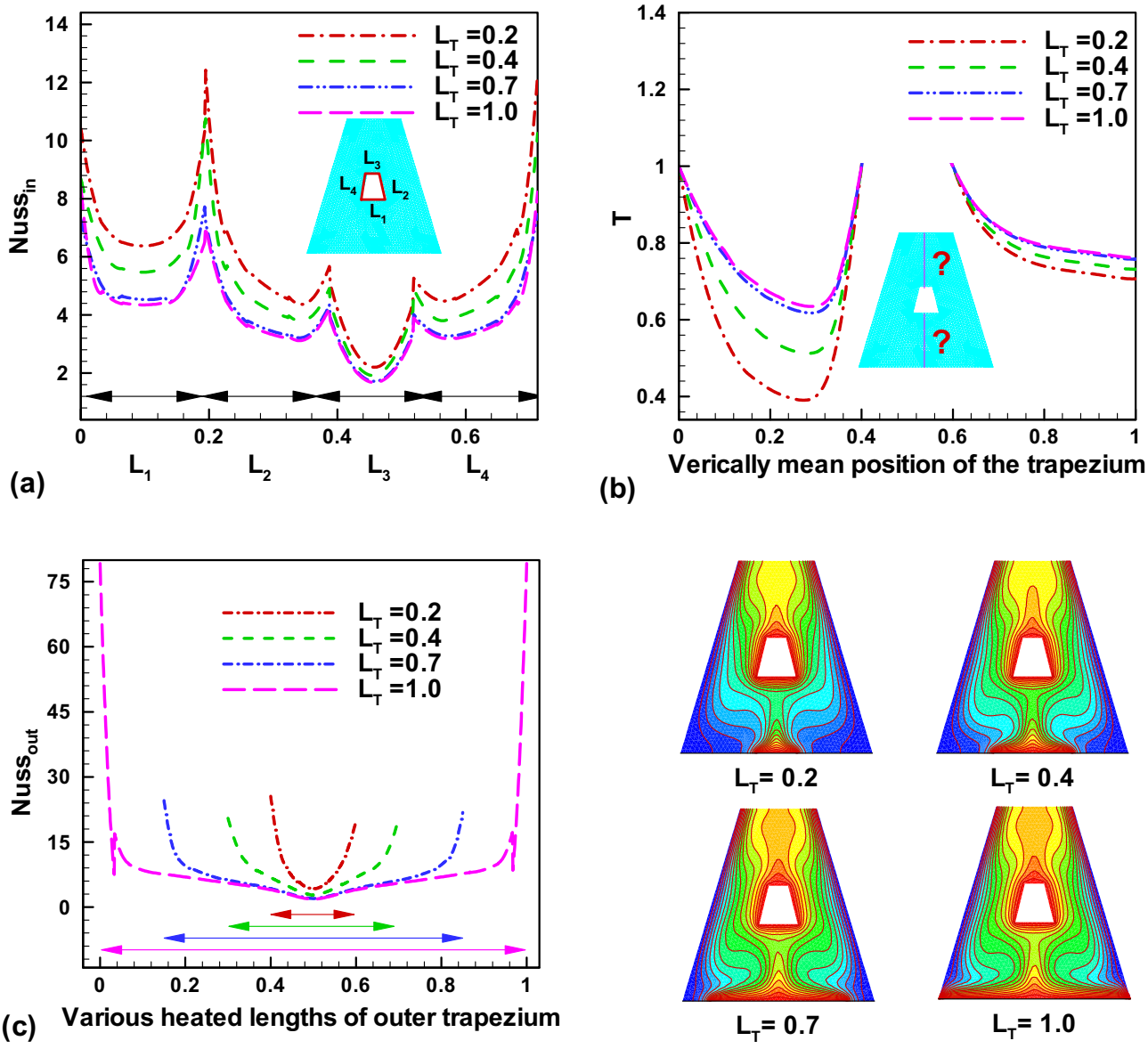

Fig. 6. Variation of (a) Nusselt number at inner cavity, (b) temperature T along the vertically mean position and (c) Nusselt number at outer heated cavity with respect to the various heated portions (L_T) of outer cavity when $Ra = 10^5$ and $\phi = 0.1$.

length of outer trapezium. Moreover, Nusselt number has higher values at the corners of each side. Fig. 6(b) shows the temperature profile variation with heated length of the bottom wall of outer trapezium. By increasing the heated length, temperature profile rises near the heated length whereas a small variation in the temperature is observed at the upper portion of the trapezium. Fig. 6(c) depicts variation of Nusselt number with heated length for the outer cavity. Nusselt number is decreasing with increasing heated length.

For various values of Rayleigh number, the streamlines for the *CuO*-water nanofluid flow are given by Fig. 7(a)-(c). The hot fluid near the inner heated cavity rises in the middle of the trapezium and falls near the cold walls which create rotation in the form of two symmetrical boluses. At higher values of *Ra* the strength of streamlines enlarges resulting in large number, size and development of the convective cells in the cavity. At $Ra = 10^4$, the streamlines are small whereas they are enlarged at higher values of $Ra = 10^5$ and $Ra = 10^{5.7}$, cover the whole cavity which shows the intensification of convective flow and heat transfer. The maximum values of stream function are 1.4033 at $Ra = 10^4$, 6.8015 at $Ra = 10^5$ and 16.415 at $Ra = 10^{5.7}$. Fig. 7(d)-(f) depicts the impact of Rayleigh number *Ra* on the temperature field of *Cu*-EG nanofluid. In Fig. 7(d) the isotherms are smooth at low Rayleigh number, showing that the convection is dominant and it induces heat transfer. The portion between the heated inner obstacle and partially heated bottom shows strong buoyancy effects while going towards the boundaries fluid temperature decreases. The convection mode is dominant for higher values of Rayleigh number, which is prominent from the hot surfaces. It is since *Ra* is the ratio of momentum and thermal diffusivity multiplied by the ratio of buoyancy and viscosity forces. The isotherms are non-smooth in Fig. 7(e) and (f). As Rayleigh number augments the distortion of the isotherm becomes larger and leads to intensify the convective flow. The buoyancy effects are stronger in the upper portion of the

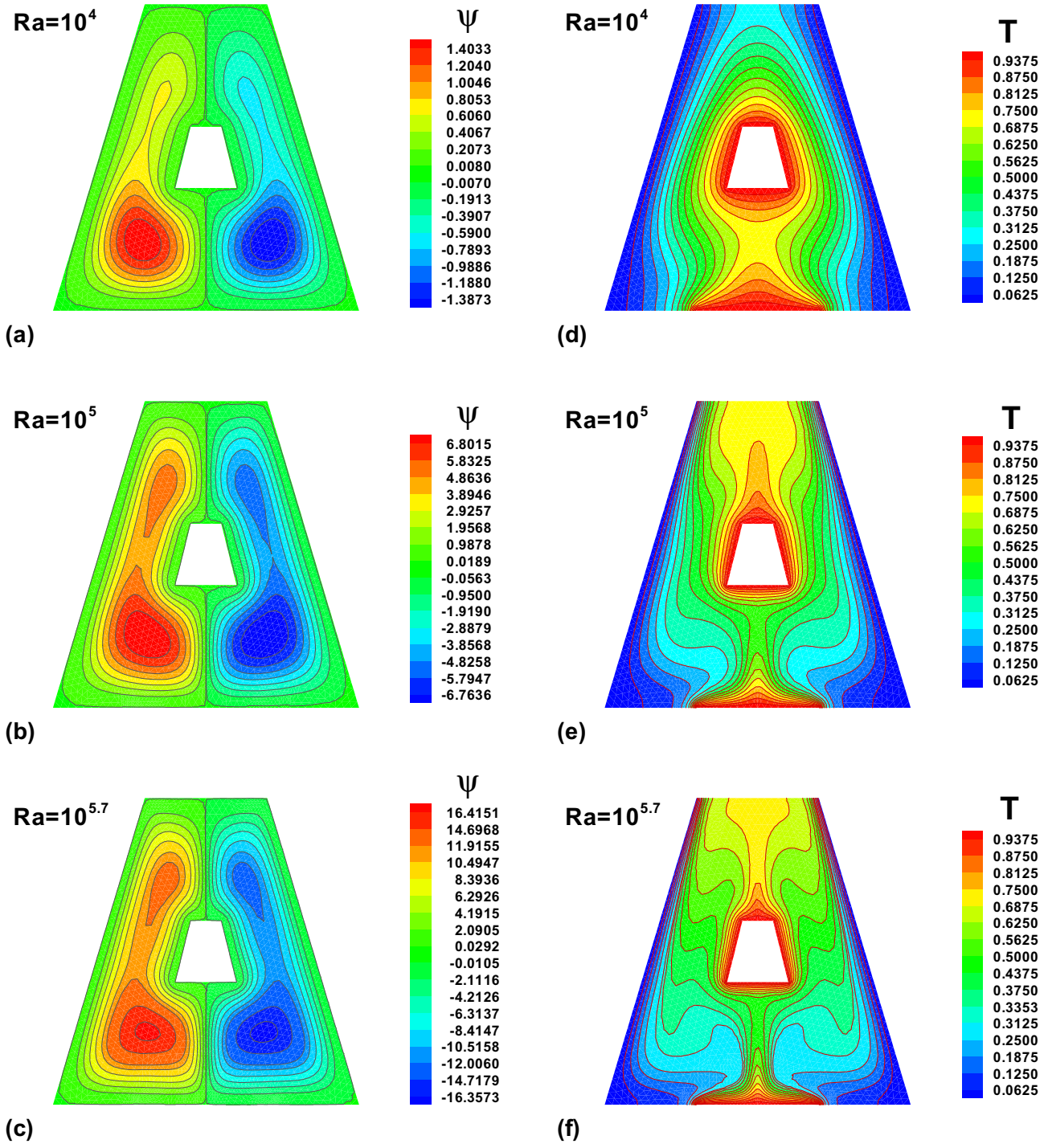

Fig. 7. Variation of (a)-(c) Stream lines ψ and (d)-(f) isotherms for various values of Rayleigh number Ra when $\phi = 0.1$. $L_T = 0.4$.

cavity and thermal plumes are generated. It is obvious in these two figures that fluid in the whole cavity becomes more heated compared to Fig. 7(d).

Fig. 8(a)-(d) shows the variation of Nusselt number, temperature and velocity with Rayleigh number. In Fig. 8(a), the Nusselt number increases with increasing Rayleigh number due to dominancy of buoyancy forces. Fig. 8(b) shows alteration of Nusselt number with Rayleigh number for different sides of inner trapezium. It can be seen that Nusselt number augments with Rayleigh number and it attains the highest value for $Ra = 10^{5.7}$.

Moreover, the highest variation is found for the bottom wall L_1 of the inner cavity. For L_2 and L_4 there is sufficient variation while at L_3 there is a small variation in Nusselt number. Fig. 8(c) and (d) shows variation of temperature and velocity distribution respectively with Rayleigh number for different mean positions (vertically) of outer trapezium. Both temperature and velocity profiles are increasing with Rayleigh number. Velocity has highest value at $Ra = 10^{5.7}$.

Fig. 9(a)-(f) depicts the behavior of streamlines and temperature with variation in ϕ for fixed value of $Ra = 10^5$ and $L_T = 0.4$.

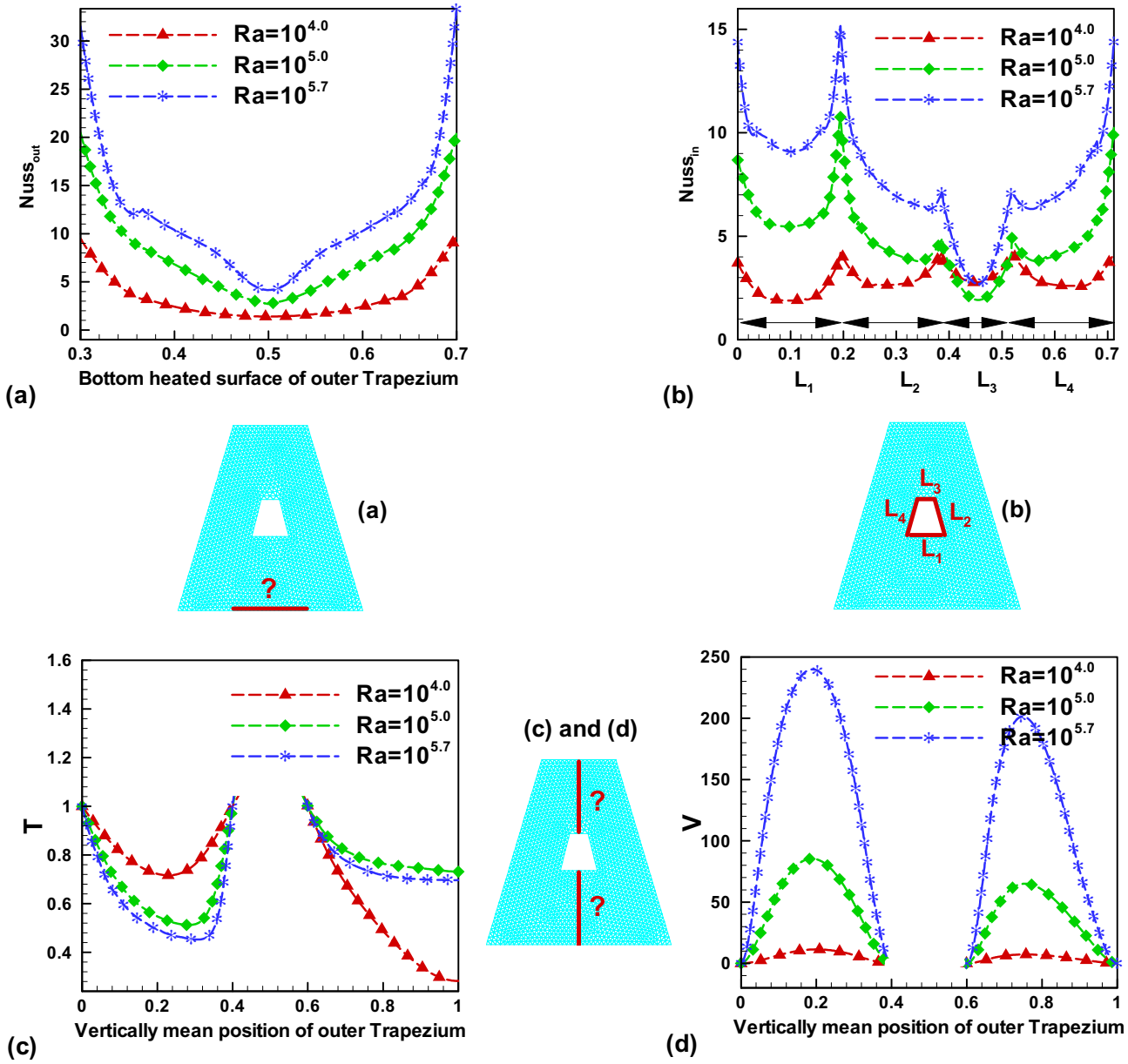

Fig. 8. Variation of (a) Nusselt number at the outer cavity, (b) Nusselt number at the inner heated cavity, (c) temperature T along vertically mean position and (d) Velocity V along vertically mean position for various values of Ra when $L_T = 0.4$ and $\phi = 0.1$.

In Fig. 9(a)-(c) the strength of streamlines becomes strong with increasing nanoparticles volume fraction and covers the whole cavity. For $Ra = 10^5$ the buoyancy effects and heat transfer are dominant, hence the smallest bolus size augments with increasing volume fraction ϕ. Two symmetric boluses are formed due to the imposed boundary conditions in the cavity. In isotherms the inner cavity is heated and bottom wall of outer cavity is partially heated. Isotherms show that fluid near the inside heated obstacle and bottom partial heated portion is hot for $\phi = 0$. For $\phi = 0.1$ and $\phi = 0.2$, thermal plumes generate near the inside obstacle due to the increase in thermal conductivity of the nanofluid. The isotherms are more contorted in Fig. 9(e) and (f).

Fig. 10(a)-(d) depicts the variation of Nusselt number, temperature and velocity with volume fraction of nanoparticles. Fig. 10(a) is considered with respect to bottom heated surface of outer trapezium and shows that Nusselt number decreases when volume fraction augments. In fact, increasing volume fraction enhances thermal conductivity and thus conduction becomes dominant which reduces Nusselt number. In Fig. 10(b), Nusselt number variation decreases with the volume fraction of nanoparticles, at side L_3 a small decrease/variation is observed while highest at L_1. Temperature profile is decreasing between the mean positions 0 and 0.25, while it enhances between 0.25 and 0.4. Temperature profile attains the highest values at mean positions 0.4 and 0.6. After crossing the inner cavity the temperature is increasing with volume fraction, depending on the mean position of outer trapezium. Velocity has lowest profile in the absence of nanoparticles and increases with volume fraction of nanoparticles.

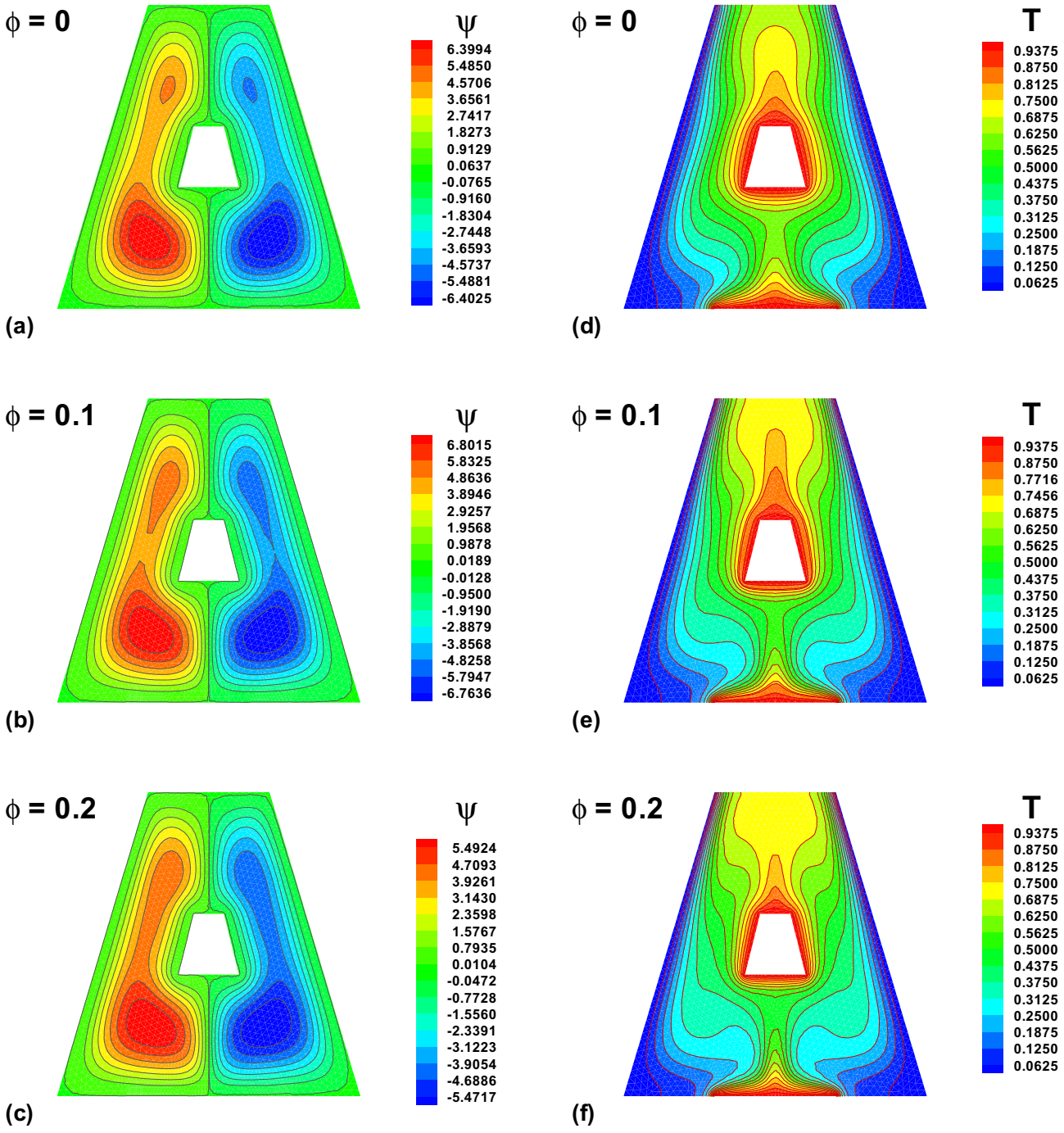

Fig. 9. Variation of (a)-(c) Stream lines ψ and (d)-(f) isotherms for various values of nanoparticles volume fraction ϕ when $Ra = 10^5$ and $L_T = 0.4$.

Fig. 11(a)-(h) shows the effect of aspect ratio AR of the inner trapezium on the streamlines and isotherms for fixed values of volume fraction $\phi = 0.1$, heated length $L_T = 1.4$ and Rayleigh number $Ra = 10^5$. It is spotted that streamlines become weak with increasing values of AR. The bolus size becomes smaller while going from $AR = 0.5$ to $AR = 3$. Isotherms show that heat dispersed in the entire cavity with the increase in values of AR. In fact, for a larger inner heated obstacle the fluid becomes hotter in the areas near inner trapezium, bottom wall and inclined walls. Heat plumes can be seen for $AR = 1$ and $AR = 2$ in the upper portion of the cavity. The isotherm maximum absolute value reaches 0.9720 for $AR = 3$.

Fig. 12(a)-(g) shows the variation of velocity profiles U and V with variation in aspect ratio AR considering the inner trapezium to be heated. As the aspect ratio AR of the inner trapezium increases, the fluid velocity U squeezes and the distortion increases. More boluses can be seen due to high value of Rayleigh number, $Ra = 10^5$.

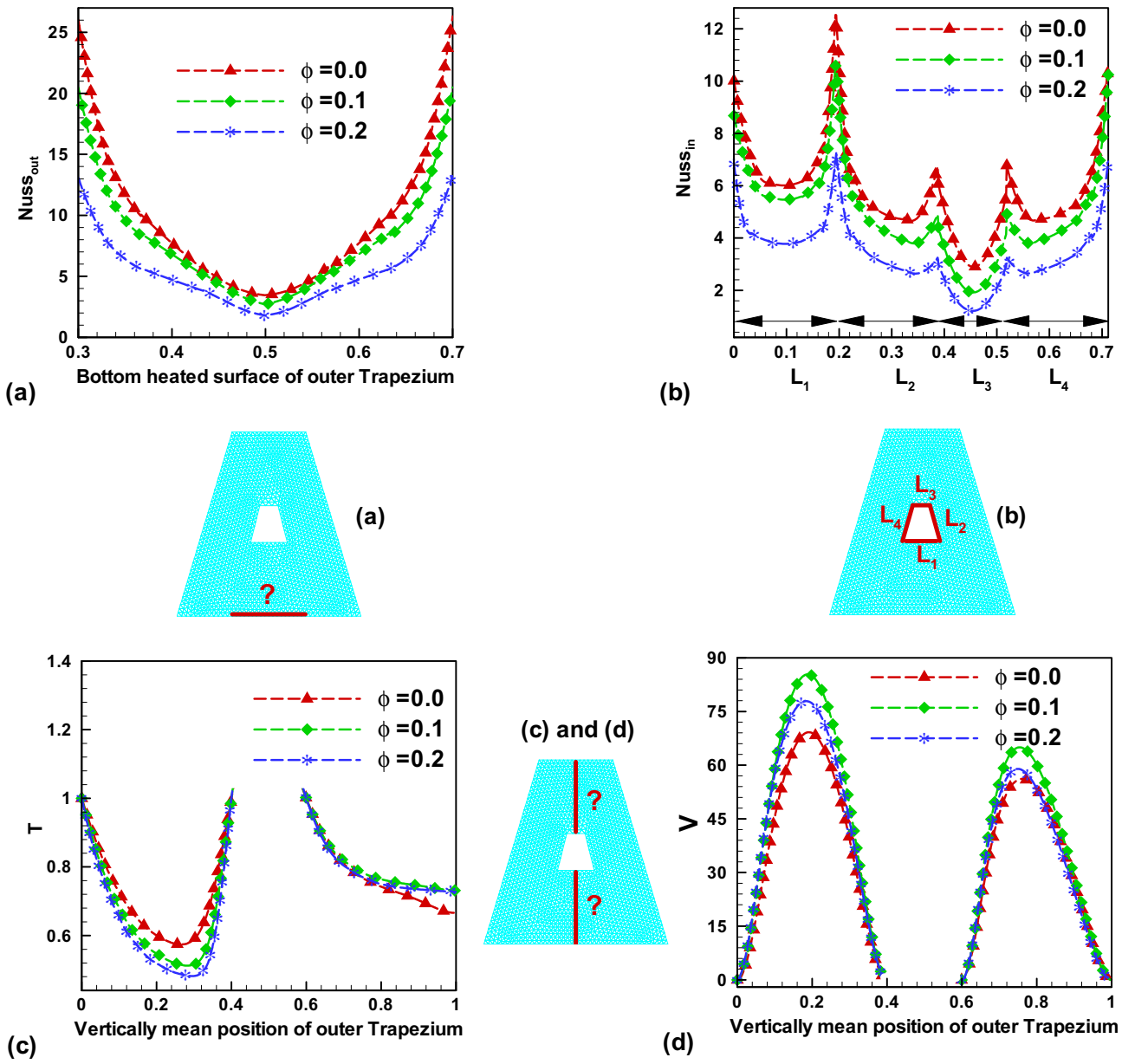

Fig. 10. Variation of (a) Nusselt number at the outer cavity, (b) Nusselt number at the inner heated cavity, (c) temperature (T) and (d) velocity (V) along vertically mean position for various values of nanoparticles volume fraction ϕ when $Ra = 10^5$ and $L_T = 0.4$.

Fig. 13(a)-(f) shows 3D presentation for the impact of three heat conditions of inner trapezium on the stream function and isotherms. The varying phenomenon of heat concerned to the nanofluid inside the cavity can be significantly observed here. The streamlines for the cold inner trapezium possess shape of two cones demonstrating that the nanofluid is hot near the bottom wall and cold in other areas. For adiabatic inner obstacle, convection is stronger than cold inner trapezium while for heated inner trapezium heat transfer is maximum. In Fig. 13(c), most of the portion of nanofluid is hot and boundary layer becomes thick. Fig. 13(d)-(f), temperature of the nanofluid increases while going from cold to heated inner trapezium. There is one heated portion for cold inner obstacle in Fig. 13(c) while heat dispersed for the adiabatic inner trapezium in Fig. 13(b). In Fig. 13(f) temperature and convection is dominant as we see two heated cloudy portions showing the dominancy of heat and convection near the inner trapezium and bottom wall of outer cavity. It makes the nanofluid hotter in the entire cavity except in small portion near the inclined cold walls where the fluid remains cold.

Fig. 14(a)-(d) shows the 3D variation of isotherms with various heated portions of outer cavity. It is evident that increasing the length of heated portion increases the heat of the nanofluid. For $L_T = 1.0$, heat dispersed in the entire cavity is showing high temperature isotherms.

5. Conclusion

In the present numerical study, the *CuO*-water nanofluid flow inside the trapezium cavity with inner heated obstacle was

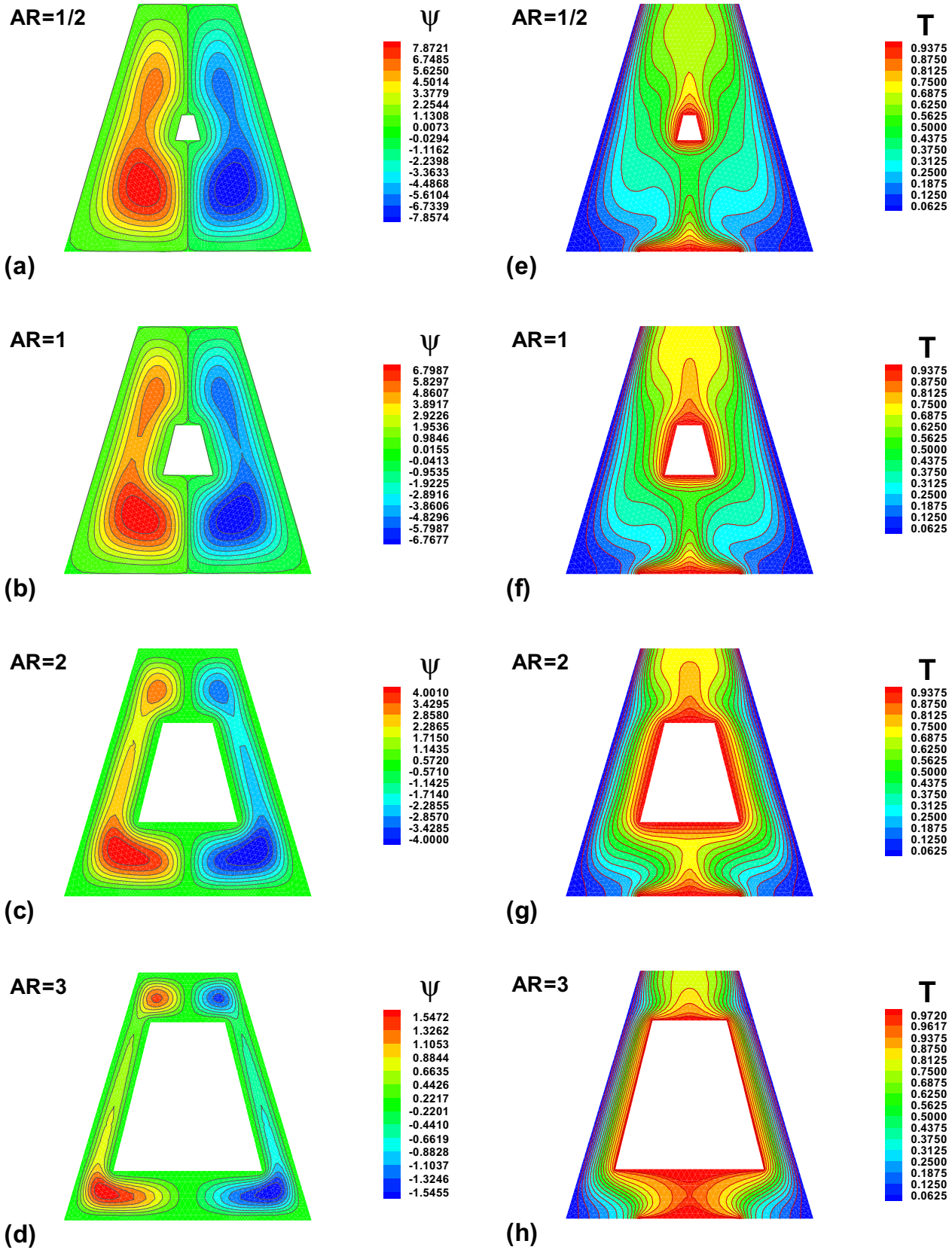

Fig. 11. Variation of (a)-(d) Stream lines ψ and (e)-(h) isotherms for different aspect ratio (AR) defined at inner size of the cavity when $L_T = 0.4, \phi = 0.1$ and $Ra = 10^5$.

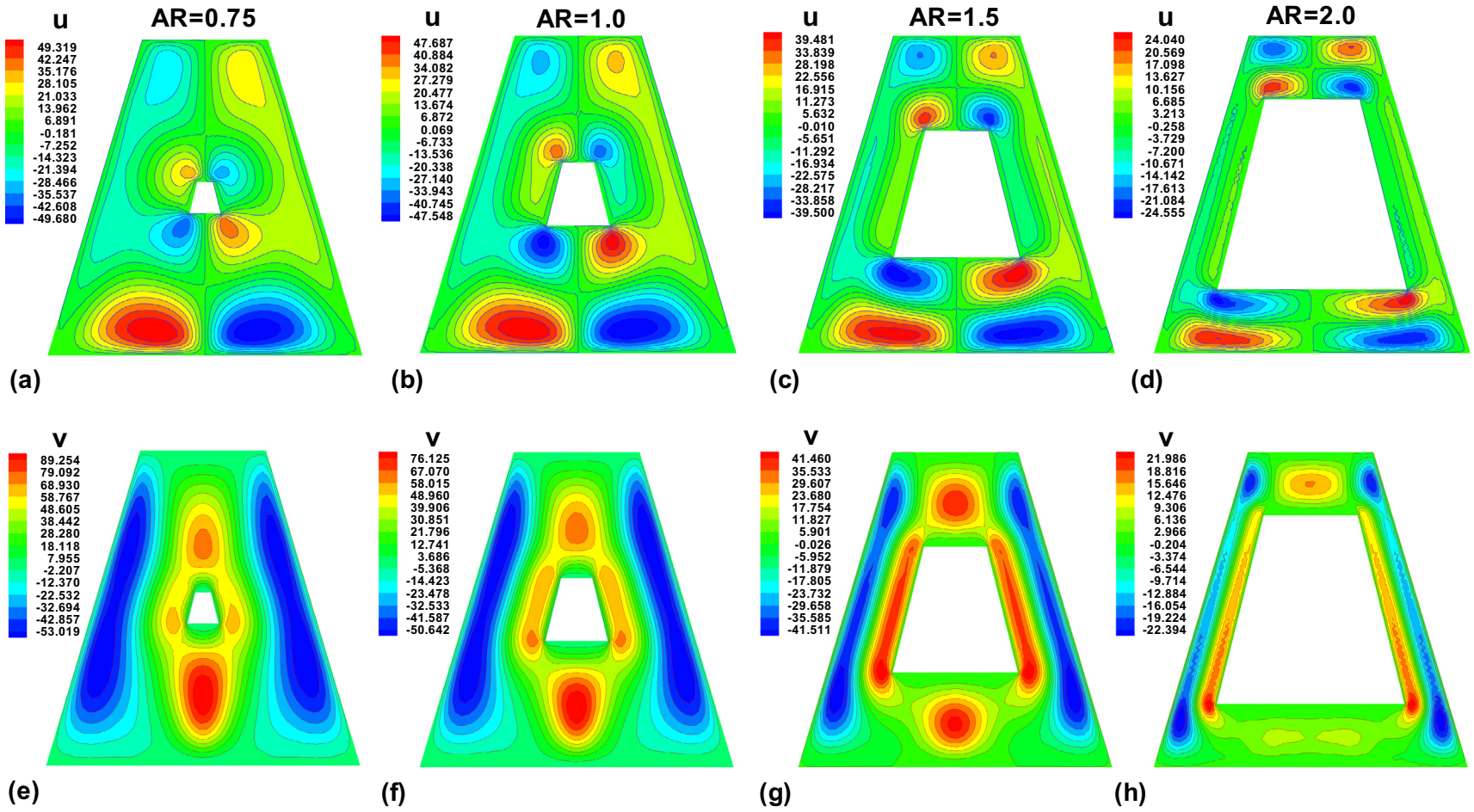

Fig. 12. Variation of velocity profiles (a)-(d) u and (e)-(h) v enclosed between the inner and outer trapezium with respect to the aspect ratios (AR) defined at inner cavity when $L_T = 0.4, \phi = 0.1$ and $Ra = 10^5$.

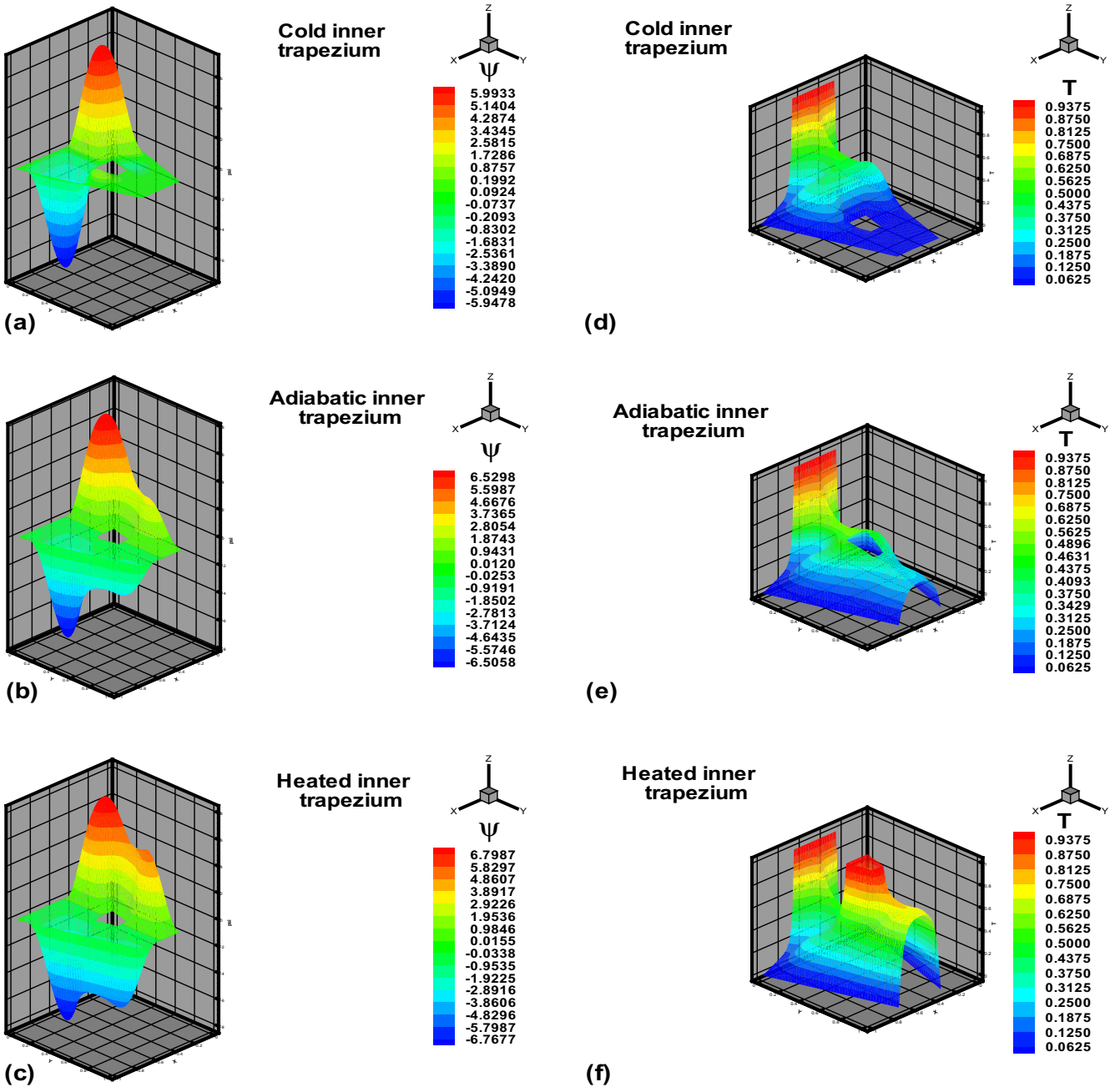

Fig. 13. Three-dimensional variation of (a)-(c) Stream lines ψ and, (d)-(f) isotherms for various conditions (cold, adiabatic and heated) defined at the inner trapezium when $L_T = 0.4, \phi = 0.1$ and $Ra = 10^5$.

investigated and the problem was solved numerically using Finite Element Method. In this model we have determine the These simulations are executed for various lengths of heated portion $(L_T = 0.2{-}1.0)$, Rayleigh number $(Ra = 10^4{-}10^{5.7})$, nanoparticles volume fraction $(\phi = 0{-}0.2)$, Aspect ratio $(AR = 0.5{-}3)$ and different kinds of inner square cylinder (cold, adiabatic and hot). It is concluded that flow field, thermal field and heat transfer rate are getting stronger due to increase in Rayleigh number. The fluid velocity is decreasing with increasing nanoparticles volume fraction ϕ as the fluid gets denser. Heat transfer rate is decreasing with the increase in ϕ and L_T due to dominant convection. For greater heated length of outer trapezium, thermal plumes generate and convection is dominant with distorted isotherms. Temperature profile is higher at the bottom of trapezium, while lower at the upper side of the inner cavity.

Conflict of interest

There is no actual or potential conflict of interest including any financial, personal or other relationships with other people or organizations.

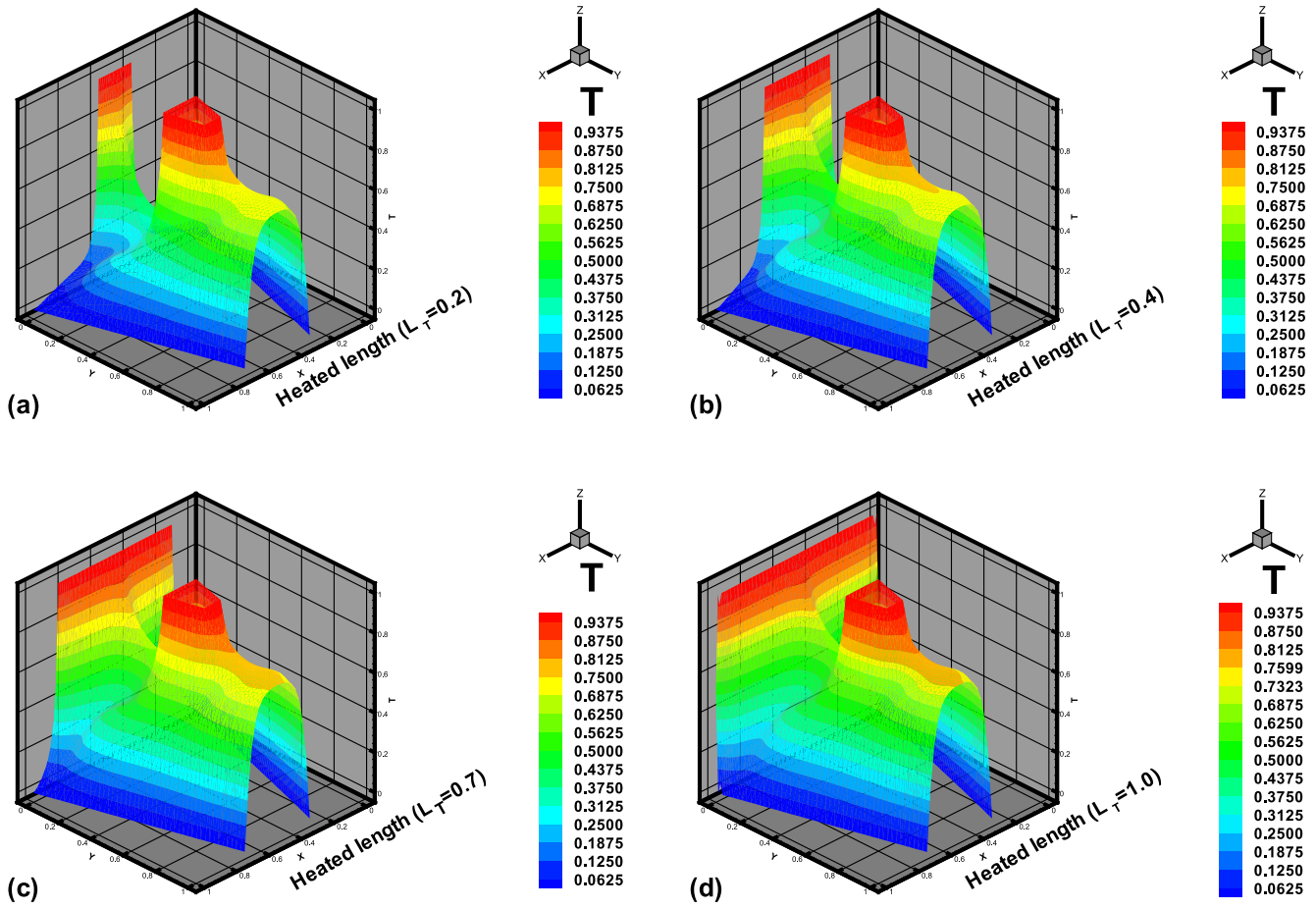

Fig. 14. Three-dimensional variation of isotherms with respect to the various heated portions (L_T) of outer cavity when $\phi = 0.1$ and $Ra = 10^5$.

Acknowledgment

Authors would like to acknowledge and express their gratitude to the United Arab Emirates University, Al Ain, UAE for providing the financial support with Grant No. 31S240-UPAR (2) 2016.

References

[1] Constantin Fetecau, Dumitru Vieru, Waqas Ali Azhar, Natural convection flow of fractional nanofluids over an isothermal vertical plate with thermal radiation, Appl. Sci. 7 (3) (2017) 247.
[2] Qasem M. Al-Mdallal, Muhammed I. Syam, P. Donald Ariel, The extended homotopy perturbation method and boundary layer flow due to condensation and natural convection on a porous vertical plate, Int. J. Comput. Math. 88 (16) (2011) 3535–3552.
[3] Milovan Perić, Natural convection in trapezoidal cavities, Numer. Heat Transfer, Part A: Appl. 24 (2) (1993) 213–219.
[4] Draco Iyi, Reaz Hasan, Natural convection flow and heat transfer in an enclosure containing staggered arrangement of blockages, Procedia Eng. 105 (2015) 176–183.
[5] V. Prasad, F.A. Kulacki, Convective heat transfer in a rectangular porous cavity—effect of aspect ratio on flow structure and heat transfer, J. Heat Transfer 106 (1) (1984) 158–165.
[6] Feng Wu, Gang Wang, Numerical simulation of natural convection in an inclined porous cavity under time-periodic boundary conditions with a partially active thermal side wall, RSC Adv. 7 (28) (2017) 17519–17530.
[7] K. Aparna, K.N. Seetharamu, Investigations on the effect of non-uniform temperature on fluid flow and heat transfer in a trapezoidal cavity filled with porous media, Int. J. Heat Mass Transfer 108 (2017) 63–78.
[8] J.C. Maxwell, Electricity and Magnetism, Clarendon Press, 1873.
[9] S.U.S. Choi, Enhancing thermal conductivity of fluids with nanoparticles, developments and applications of non-Newtonian flows, ASME FED 105 (99) (1995) 231.
[10] Phillbot Keblinski, S.R. Phillpot, S.U.S. Choi, J.A. Eastman, Mechanisms of heat flow in suspensions of nano-sized particles (nanofluids), Int. J. Heat Mass Transfer 45 (4) (2002) 855–863.
[11] Sidra Aman, Ilyas Khan, Zulkhibri Ismail, Mohd Zuki Salleh, Qasem M. Al-Mdallal, Heat transfer enhancement in free convection flow of CNTs Maxwell nanofluids with four different types of molecular liquids, Sci. Rep. 7 (1) (2017) 2445.
[12] Sidra Aman, Ilyas Khan, Zulkhibri Ismail, Mohd Zuki Salleh, Ali Saleh Alshomrani, Metib Said Alghamdi, Magnetic field effect on Poiseuille flow and heat transfer of carbon nanotubes along a vertical channel filled with Casson fluid, AIP Adv. 7 (1) (2017) 015036.
[13] Zoubair Boulahia, Abderrahim Wakif, Rachid Sehaqui, Mixed convection heat transfer of Cu-water nanofluid in a lid driven square cavity with several heated triangular cylinders, Int. J. Innovat. Appl. Stud. 17 (1) (2016) 82.
[14] Rizwan Ul Haq, S. Naveed Kazmi, Toufik Mekkaoui, Thermal management of water based SWCNTs enclosed in a partially heated trapezoidal cavity via FEM, Int. J. Heat Mass Transfer 112 (2017) 972–982.
[15] Fatih Selimefendigil, Hakan F. Öztop, Ali J. Chamkha, Analysis of mixed convection of nanofluid in a 3D lid-driven trapezoidal cavity with flexible side surfaces and inner cylinder, Int. Commun. Heat Mass Transfer 87 (2017) 40–51.
[16] M. Alinia, D.D. Ganji, M. Gorji-Bandpy, Numerical study of mixed convection in an inclined two-sided lid-driven cavity filled with nanofluid using two-phase mixture model, Int. Commun. Heat Mass Transfer 38 (10) (2011) 1428–1435.
[17] Mohsen Sheikholeslami, Houman B. Rokni, Melting heat transfer influence on nanofluid flow inside a cavity in existence of magnetic field, Int. J. Heat Mass Transfer 114 (2017) 517–526.
[18] Mohsen Sheikholeslami, Mohammadkazem Sadoughi, Mesoscopic method for MHD nanofluid flow inside a porous cavity considering various shapes of nanoparticles, Int. J. Heat Mass Transfer 113 (2017) 106–114.
[19] Farhad Talebi, Amir Houshang Mahmoudi, Mina Shahi, Numerical study of mixed convection flows in a square lid-driven cavity utilizing nanofluid, Int. Commun. Heat Mass Transfer 37 (1) (2010) 79–90.
[20] Zoubair Boulahia, Abderrahim Wakif, Rachid Sehaqui, Numerical investigation of mixed convection heat transfer of nanofluid in a lid driven square cavity with three triangular heating blocks, Int. J. Comput. Appl. 143 (6) (2016) 37–45.
[21] Nader Ben-Cheikh, Ali J. Chamkha, Brahim Ben-Beya, Taieb Lili, Natural convection of water-based nanofluids in a square enclosure with non-uniform heating of the bottom wall, J. Mod. Phys. 4 (02) (2013) 147.

[22] Mohammad Hemmat Esfe, Ali Akbar Abbasian Arani, Wei-Mon Yan, Hamidreza Ehteram, Alireza Aghaie, Masoud Afrand, Natural convection in a trapezoidal enclosure filled with carbon nanotube–EG–water nanofluid, Int. J. Heat Mass Transfer 92 (2016) 76–82.
[23] Victor M. Job, Sreedhara Rao Gunakala, Mixed convection nanofluid flows through a grooved channel with internal heat generating solid cylinders in the presence of an applied magnetic field, Int. J. Heat Mass Transfer 107 (2017) 133–145.
[24] Ali Khaleel Kareem, Shian Gao, Ahmed Qasim Ahmed, Unsteady simulations of mixed convection heat transfer in a 3D closed lid-driven cavity, Int. J. Heat Mass Transfer 100 (2016) 121–130.
[25] Feroz Ahmed Soomro, Z. Hammouch, Heat transfer analysis of CuO-water enclosed in a partially heated rhombus with heated square obstacle, Int. J. Heat Mass Transfer 118 (2018) 773–784.
[26] Muneer A. Ismael, Eiyad Abu-Nada, Ali J. Chamkha, Mixed convection in a square cavity filled with CuO-water nanofluid heated by corner heater, Int. J. Mech. Sci. 133 (2017) 42–50.
[27] M. Khan, R. Ali, A. Shahzad, MHD Falkner-Skan flow with mixed convection and convective boundary conditions, Walailak J. Sci. Technol. (WJST) 10 (5) (2013) 517–529.
[28] A. Sokolov, R. Ali, S. Turek, An AFC-stabilized implicit finite element method for partial differential equations on evolving-in-time surfaces, J. Comput. Appl. Math. 289 (2014) 101–115.
[29] J. Ahmed, A. Shahzad, M. Khan, R. Ali, A note on convective heat transfer of an MHD Jeffrey fluid over a stretching sheet, AIP Adv. 5 (11) (2015) 117117.
[30] T. Aziz, F.M. Mahomed, A. Shahzad, R. Ali, Travelling wave solutions for the unsteady flow of a third grade fluid induced due to impulsive motion of flat porous plate embedded in a porous medium, J. Mech. 30 (05) (2015) 527–535.
[31] R. Ali, A. Shahzad, M. Khan, M. Ayub, Analytic and numerical solutions for axisymmetric flow with partial slip, Eng. Comput. 32 (1) (2016) 149–154.
[32] M. Usman, T. Zubair, M. Hamid, Rizwan Ul Haq, Wei Wang, Cu-Al_2O_3/water hybrid nanofluid through a permeable surface presence of nonlinear radiation and variable thermal conductivity via LSM, Int. J. Heat Mass Transfer 126 (2018) 1347–1356.
[33] Feroz Ahmed Soomro, M. Usman, Rizwan Ul Haq, W. Wang, Melting heat transfer analysis of Sisko fluid over a moving surface with nonlinear thermal radiation via collocation method, Int. J. Heat Mass Transfer 126 (2018) 1034–1042.
[34] M. Usman, T. Zubair, M. Hamid, Rizwan Ul Haq, Wei Wang, Shape effects of MoS2 nanoparticles on rotating flow of nanofluid along a stretching surface with variable thermal conductivity: a Galerkin Approach, Int. J. Heat Mass Transfer 124 (2018) 706–714.
[35] M. Usman, Feroz Ahmed Soomro, Rizwan Ul Haq, W. Wang, Ozlem Defterli, Thermal and velocity slip effects on Casson nanofluid flow over an inclined permeable stretching cylinder via collocation method, Int. J. Heat Mass Transfer 122 (2018) 1255–1263.
[36] Rizwan Ul Haq, F.A. Soomro, Toufik Mekkaoui, Qasem M. Al-Mdallal, MHD natural convection flow enclosure in a corrugated cavity filled with a porous medium, Int. J. Heat Mass Transfer 121 (2018) 1168–1178.
[37] Muhammad Usman, Muhammad Hamid, Rizwan Ul Haq, Wei Wang, Heat and fluid flow of water and ethylene-glycol based Cu-nanoparticles between two parallel squeezing porous disks: LSGM approach, Int. J. Heat Mass Transfer 123 (2018) 888–895.
[38] Rizwan Ul Haq, Feroz Ahmed Soomro, Zakia Hammouch, Heat transfer analysis of *CuO*-water enclosed in a partially heated rhombus with heated square obstacle, Int. J. Heat Mass Transfer 118 (2018) 773–784.
[39] Junemoo Koo, Clement Kleinstreuer, A new thermal conductivity model for nanofluids, J. Nanopart. Res. 6 (6) (2004) 577–588.
[40] James Clerk Maxwell, A Treatise on Electricity and Magnetism, Oxford University Press, H. Milford, 1937.
[41] H.C. Brinkman, The viscosity of concentrated suspensions and solutions, J. Chem. Phys. 20 (4) (1952), 571–571.
[42] Jie Li, Computational analysis of nanofluid flow in microchannels with applications to micro-heat sinks and bio-MEMS, PhD Thesis NC State University, Raleigh, NC, the United States; 2008.
[43] Cedric Taylor, Paul Hood, A numerical solution of the Navier-Stokes equations using the finite element technique, Comput. Fluids 1 (1) (1973) 73–100.